Applied Catalysis B: Environmental 136–137 (2013) 70–80

Contents lists available at SciVerse ScienceDirect

Applied Catalysis B: Environmental

journal homepage: www.elsevier.com/locate/apcatb

Influence of the preparation method and dopants nature on the WGS activity of gold catalysts supported on doped by transition metals ceria

T. Tabakova[a,*], L. Ilieva[a], I. Ivanov[a], R. Zanella[b], J.W. Sobczak[c], W. Lisowski[c], Z. Kaszkur[c], D. Andreeva[a]

[a] Institute of Catalysis, Bulgarian Academy of Sciences, Acad. G. Bonchev St., Block 11, 1113 Sofia, Bulgaria
[b] Centro de Ciencias Aplicadas y Desarrollo Tecnológico Universidad Nacional Autónoma de México, Circuito Exterior S/N, Ciudad Universitaria.C. P. 04510 México D.F., Mexico
[c] Institute of Physical Chemistry, PAS, Kasprzaka 44/52, 01-224 Warsaw, Poland

ARTICLE INFO

Article history:
Received 18 September 2012
Received in revised form 13 January 2013
Accepted 19 January 2013
Available online 9 February 2013

Keywords:
Gold catalysts
WGSR
Ceria doped by Fe, Mn and Sn oxides

ABSTRACT

Gold catalysts supported on ceria doped by different metal oxides (Me = Fe, Mn, Sn) were synthesized by two different methods: coprecipitation (CP) and mechanochemical activation (MA). Samples were characterized by means of XRD, HRTEM, TPR and XPS. Both XRD and HRTEM analyses reveal differences in the average size of the gold and ceria particles. As shown by TPR data, ceria doping improves oxygen mobility, i.e. a higher oxygen capacity was observed while compared with gold catalyst on undoped ceria. The method of preparation and the nature of dopant applied influence the catalytic performance in the water–gas shift (WGS) reaction. The differences in WGS activity between the MA and CP samples were significant. The MA catalysts, doped by Fe and Mn, manifested higher WGS activity than the undoped Au/ceria sample and the sample doped by Sn. A high concentration of Ce^{3+} ions in the highly active catalysts containing Fe or Mn was registered by XPS and found consistent with an earlier proposed model of the active sites for the WGS reaction.

1. Introduction

Gold catalysts based on ceria have been found very promising for the water–gas shift (WGS) reaction because of their high activity at low and medium temperatures [1–21]. During the past decade, there was growing interest in this reaction due to the advancement in fuel cells technology and the related hydrogen fuel processing. Supported gold catalysts have some advantageous features (stable in oxidizing atmosphere, non-pyrophoric, use without preliminary activation) in comparison with conventionally applied $Cu/ZnO/Al_2O_3$ LT-WGS catalyst. However, in addition to the high catalytic activity, the WGS gold catalysts should demonstrate good stability under cyclic working conditions. The nature of the support on which nanosized gold particles are dispersed plays a crucial role in determining the catalytic performance. In this context, ceria is a very good choice to support gold catalysts. Its suitability is mainly due to the ability to shift easily between reduced and oxidized state ($Ce^{3+} \leftrightarrow Ce^{4+}$), which results in rapid formation and elimination of oxygen vacancy defects. An additional advantage of ceria is the stabilization of the active metal phase in a highly dispersed state. Modification of the ceria support by doping metals of lower oxidation state (below 4+) affects redox properties and gives rise to the formation of oxygen vacancies in the ceria crystal structure that also increase the oxygen capacity of the ceria-based catalysts [22]. The use of different dopants and different preparation methods for synthesis of ceria-based materials as supports for gold catalysts can strongly influence their catalytic performance. Recently, gold catalysts supported on ceria doped by Al^{3+} as well as by different rare earth (RE) metals (La, Sm, Gd, Y, Yb) have been synthesized [23–26]. The effect of the dopant nature and preparation method on the WGS activity was studied. A higher catalytic activity of samples prepared by mechanochemical activation (MA) in comparison with materials synthesized by a coprecipitation method (CP) has been reported. The catalytic activity of gold catalyst on ceria modified by alumina (10 wt%), prepared by the MA mode, was close to that of gold on undoped ceria [24]. Ceria-based catalysts doped by Sm and Yb manifested high WGS activity showing a better performance compared to gold on ceria [26]. In addition, a stabilization of gold and ceria dispersion against agglomeration in the presence of alumina or RE metal oxides was observed. Another reason of deactivation was connected with the formation of carbonates or formates on the catalyst surface and with blocking the active sites

* Corresponding author. Tel.: +359 2 979 25 28; fax: +359 2 971 29 67.
E-mail addresses: tabakova@ic.bas.bg, ttabakova@yahoo.com (T. Tabakova).

0926-3373/$ – see front matter © 2013 Elsevier B.V. All rights reserved.
http://dx.doi.org/10.1016/j.apcatb.2013.01.050

[15,27–30]. The increase of ceria oxygen capacity should prevent the build-up of carbonate species on the surface and as a result could increase the stability of the catalysts.

So far, scarce results have been reported on the use of ceria doped by Fe, Mn, and Sn as supports of gold catalysts in the WGS reaction. Different preparation methods have been used by Wang and Gorte to test the role of Fe as a dopant for improvement of the WGS activity over Pd/CeO_2 [31]. A significant rate enhancement has been observed after deposition of monolayer of Fe_2O_3 on ceria by impregnation in comparison to the catalyst with Fe-ceria prepared by sol–gel method, in which Fe was in the bulk of the ceria. The use of mixed Ce-Fe oxides (25, 50 and 75 wt% Fe_2O_3) as support of gold catalysts has revealed strong influence of the support composition on the catalytic performance in the WGSR and preferential CO oxidation (PROX) reactions [32,33]. The effect has been attributed to significant difference in gold particles size and in the ability of the supports to assist oxygen vacancies formation. The beneficial influence of ceria doping with Fe on total and preferential CO oxidation of gold catalysts has been recently reported [34,35]. The modification of ceria by Fe facilitated high gold dispersion by creating sites with an increased electronic density. The synergy Au–Ce–Fe and the enhanced reducibility have been invoked to explain improved catalytic performance. Doping of ceria with Fe and Mn by mechanochemical activation route has been shown as the most promising approach for synthesis of active and selective gold catalysts for PROX reaction [36]. The differences in catalytic behaviour have been related to supports' structural peculiarities, since high dispersion of gold particles was evidenced by HRTEM. Recent studies have shown that high CO oxidation activity during the PROX reaction could be also achieved after deposition of gold nanoparticles on α-Mn_2O_3 [37] or MnO_2-CeO_2 [38]. Wang et al. have found that the CO oxidation activity of Au/SnO_2 catalysts is dependent on both the particle size and the degree of crystallinity of the tin dioxide support [39].

In the present paper, we report results on the WGS activity of gold catalysts supported on ceria doped by different metals (Fe, Mn, Sn). The catalysts were characterized by means of XRD, HRTEM, TPR and XPS. Emphasis is given on the relationship between the structure and properties of the catalysts and their catalytic activity. The role of the preparation method and dopant nature is also discussed.

2. Experimental

2.1. Sample preparation

Mixed CeO_2-Me_xO_y (Me = Fe, Mn, Sn) supports were prepared by two different techniques. One of them was a coprecipitation method (CP). The initial salts of the dopants were $Fe(NO_3)_3.9H_2O$, $Mn(NO_3)_2{\cdot}4H_2O$, and $SnCl_2{\cdot}2H_2O$. A mixed solution of $Ce(NO_3)_3{\cdot}6H_2O$ and the corresponding metal nitrate at a desired ratio (10 wt% of dopant) was co-precipitated with a solution of K_2CO_3 at constant pH 9.0 and at a temperature of 60 °C. These conditions led to a complete coprecipitation. The resulting precursors were aged at the same temperature for 1 h, then filtered and carefully washed until removal of NO_3^- or Cl^- ions. The washed precipitates were dried in vacuum at 80 °C and calcined in air at 400 °C for 2 h. The samples prepared in this way are denoted as follows: CeFeCP, CeMnCP, and CeSnCP.

The second technique used for catalyst preparation was a mechanochemical activation (MA) procedure. The mixed oxide support was prepared by mechanical mixing of the corresponding metal oxide (Fe_2O_3, MnO_2, SnO_2) and freshly prepared vacuum-dried cerium hydroxide. Cerium hydroxide was synthesized from aqueous solutions of $Ce(NO_3)_3{\cdot}6H_2O$ and K_2CO_3 under the conditions described above. The same precipitation method and thermal treatment was employed for synthesis of metal oxides (Fe_2O_3, MnO_2, SnO_2), starting from the above mentioned initial salts. A mixture of cerium hydroxide and the corresponding Me_xO_y was subjected to mechanochemical milling for 30 min in a mortar and calcination at 400 °C for 2 h. The content of Me_xO_y was 10 wt%. Prior to the final deposition of the Au^{3+} complexes, the mixed oxide support was activated in a UV disintegrator under vigorous stirring. The samples prepared in this way are denoted as follows: CeFeMA, CeMnMA, and CeSnMA.

Gold (3 wt%) was introduced by deposition–precipitation method. Gold was deposited as $Au(OH)_3$ on a mixed metal oxide support preliminary suspended in water. The precipitation was carried out by means of 'Contalab' system (Switzerland) under full control of all parameters of preparation (pH, temperature, stirring speed, reactant feed flow rates, etc.). The details are given in Ref. [2]. After filtering and careful washing, the precursors were dried under vacuum and calcined in air at 400 °C for 2 h. The gold-containing samples were denoted as AuCeFeCP, AuCeMnCP, AuCeSnCP and AuCeFeMA, AuCeMnMA, AuCeSnMA, prepared by co-precipitation and mechanochemical activation, respectively.

An undoped Au/CeO_2 sample, used as a reference, was prepared also by deposition–precipitation method under the conditions described above. All initial salts used were 'analytical grade'.

2.2. Sample characterization

The BET surface area of the samples was determined on a Micromeritics 'Flow Sorb II-2300' device. Prior to the measurements, the samples were outgassed at 200 °C for 30 min under vacuum.

The actual gold loading for each catalyst was 3 (±0.05) wt%, as measured by Atomic Absorption spectroscopy.

X-ray diffraction measurements were performed using Siemens D5005 diffractometer (Bruker-AXS), Cu sealed tube operating at 40 kV and 40 mA, and scintillation detector. Data analysis had to be conducted with care as some of the samples (CP) were found to be forced by anisotropic strain affecting not only peak broadening but also peak position of CeO_2. For a proper estimation of the lattice parameter we had thus to modify a conventional method of lattice parameter extrapolation. The latter involved 11 measured reflections of ceria.

High-resolution transmission electron microscopy (HRTEM) observations combined with Z-contrast (also called high-angle annular dark field (HAADF)) analysis of the catalysts were performed using a JEM 2010 FasTem analytical microscope equipped with a Z-contrast annular detector. Histograms of the metal particle sizes were acquired by the measurement of more than 700 particles obtained by Z-contrast and thermal diffuse scattering (TDS) observations. It should be emphasized that the HAADF technique allows to observe the gold particles selectively because other doped metals are very light in comparison with Au and Ce to produce a bright zone.

XPS spectra were registered on a PHI 5000 VersaProbe scanning ESCA Microprobe using monochromatic Al Kα radiation ($h\nu$ = 1486.6 eV) from an X-ray source operating at 200 μm spot size, 50 W and 15 kV. The analyzer pass energy was 23.5 eV, an electron take off angle was 80° and the energy step size was 0.05 eV for the Au 4f XP spectra and 0.1 eV for other elements. Before analysis, the samples were pressed into thin wafers and degassed in a preparation chamber. The Shirley background subtraction and peak fitting with Gaussian-Lorentzian product peak was performed using an Avantage XPS processing program (Thermo Electron Corporation). The charging effects were corrected by adjusting the $Ce3d_{3/2}$ peak, usually described as u''' peak to a position of 917.00 eV [40–42].

TPR measurements were carried out by means of an apparatus described elsewhere [43]. A cooling trap (−40 °C) for removing water formed during reduction was mounted in the gas line prior to the thermal conductivity detector. A hydrogen-argon mixture (10% H_2), dried over a molecular sieve 5A (−40 °C), was used to reduce the samples at a flow rate of 24 mL min^{-1}. The temperature was linearly raised at a rate of 15 °C min^{-1}. Each sample used weighed about 0.05 g. This was selected by the criterion proposed by Monti and Baiker [44]. Hydrogen consumption during the reduction process was calculated using preliminary calibration of the thermal conductivity detector, performed by reducing different amounts of NiO to Ni (NiO–'analytical grade', calcined at 800 °C for 2 h to avoid the presence of non-stoichiometric oxygen).

2.3. Catalytic activity measurements

The catalytic activity of the samples in the WGS reaction, expressed as the degree of CO conversion, was evaluated over a wide temperature range (140–350 °C). The activity was measured in a flow reactor at atmospheric pressure. A gas mixture of initial composition 4.5 vol.% CO in argon was used. The WGS reaction was performed under the following experimental conditions: catalyst bed volume–0.5 cm^3 (0.63–0.80 mm sieve fraction), space velocity of the dry gas (GHSV) = 4000 h^{-1}, partial pressure of water vapour–31.1 kPa.

Prior to the catalytic measurements, the samples were treated in a flowing air at 200 °C for 60 min at space velocity 2000 h^{-1}, followed by cooling down to the initial reaction temperature in air. Carbon monoxide content at the reactor outlet was determined using an Uras 3G (Hartmann&Braun AG) gas analyzer.

Stability tests with the AuCeFeMA catalyst were conducted at 250 °C and GHSV = 4000 h^{-1} keeping the sample under reaction conditions for 40 h (8 h a day for a period of 5 days). During pauses, the reaction mixture was kept at room temperature.

3. Results and discussion

3.1. Catalyst characterization

The effect of the preparation method on the catalysts specific surface area is demonstrated in Table 1. Coprecipitation route results in catalysts with slightly lower S_{BET}. The values are close to the surface area of Au/ceria (88 m^2 g^{-1}) and correlate with below reported data for incorporation of dopant ions in ceria cell. A similar trend of decreased surface area with increased amount of Fe_2O_3 in mixed Ce-Fe oxides, prepared by coprecipitation was reported by Bao et al. [45]. A tendency of increase of specific surface area was observed for MA-prepared gold catalysts on ceria doped by Fe and Mn. No clear effect of the nature of dopant can be registered.

The XRD patterns of all studied catalysts are presented in Fig. 1. Based on XRD measurements of the studied catalysts, the lattice parameters, depending on the dopants applied, were calculated. The average size of the gold and ceria particles was also estimated. Due to effects of strain deduced from experimental data, both particle sizes and lattice parameters had to be determined with proper account for the strain. The overall isotropic strain parameter was determined together with particle sizes following the Williamson-Hall plot scheme [46]. The samples micro-strain comes from the analysis of Williamson-Hall plot, and thus from angular dependence of peak broadening and can be hardly visible from the diffraction pattern plot. At the same time the rate of intensity attenuation of the higher angle peaks with diffraction angle (in respect to theoretical intensities) is indicative of the range of displacements of the phase atoms from the lattice nodes. All these data can help in assessment of the disorder phenomena. The lattice parameters of the MA samples were estimated by linear extrapolation of the lattice constant values from 11 individual reflections. The extrapolation was done on lattice parameter versus cosine of the Bragg angle diagram by calculating intercept of the best fit straight line with y-axis. These data showed good linearity. With the CP samples the linearity was unsatisfactory, the scattering being correlated with the observed strain parameter. For these data, extrapolation was not reliable and the lattice parameters were estimated from the average differences between the MA and CP samples assuming that the experimental error affects both kinds of samples in the same way. The data are summarized in Table 1. The X-ray diffractograms show the diffraction lines of CeO_2 that are typical of the cubic crystal structure of fluorite type oxide. With the MA samples, one can observe a small amount of a second phase due to applied dopant: Fe_2O_3 and SnO_2 for the AuCeFeMA and AuCeSnMA samples, respectively. However, this second phase was not detectable with the AuCeMnMA sample. The different preparation methods influence slightly the average size of ceria. The calculations show that in the MA samples it was higher (10–12 nm) than that in the CP samples (6–9 nm). The same trend in the average ceria particles size was observed in our previous investigation of gold catalysts supported on ceria doped by Al or RE metal [25,26], thus evidencing good reproducibility of applied preparation methods.

Analyzing the data on calculated lattice parameters it can be concluded that, owing to incorporated dopant, ceria lattice is slightly contracted. It should be noted, that all the dopants have lower ionic radii than that of Ce^{+4} (0.97 Å). Further, the CP samples demonstrate tendency for lower values of parameter a, evidencing a deep incorporation of dopant by the applied CP method and formation of solid solution. The strain is maximal for the AuCeFeCP sample. Likely, Fe occurs in the (3+) oxidation state and its incorporation into the ceria lattice should cause oxygen vacancy formation. Clearly, iron is a major source of the overall strain. On the other hand, both Sn and Mn can be in the (4+) oxidation state and can fit into the octahedral oxygen neighbourhood affecting only the size of the octahedra.

Very weak reflections at $2\Theta = 38.2°$, typical of metallic Au (1 1 1), are observed in the X-ray difractograms of the CP catalysts, as well as in that of Au/Ce. The average crystallite size of gold calculated from the X-ray line broadening using the Scherrer's equation showed similar values for the doped-ceria catalysts: 2.9 nm for AuCeMnCP and AuCeSnCP and 3.3 nm for AuCeFeCP (Table 1). In contrast, diffraction lines of gold could not be detected in the

Table 1
BET surface area, lattice parameters of ceria, average size of ceria and gold particles, measured by XRD (* – measured by HRTEM).

Samples	S_{BET}, (m^2 g^{-1})	Lattice parameter of CeO_2 a (Å)	Average size of CeO_2 (nm)	Average size of Au (nm)
AuCe	88.0	5.417 ± 0.003	11.5 ± 1	6.5 ± 0.2 (*<1/10)
AuCeFeCP	87.0	5.394 ± 0.003	9.4 ± 1	3.3 ± 0.2 (*2.8)
AuCeMnCP	82.0	5.394 ± 0.003	6.3 ± 1	2.9 ± 0.2 (*2.9)
AuCeSnCP	84.0	5.391 ± 0.003	7.4 ± 1	2.9 ± 0.2
AuCeFeMA	90.0	5.404 ± 0.003	10.1 ± 1	n.d. (*2.5)
AuCeMnMA	95.0	5.399 ± 0.003	10.7 ± 1	2.9 ± 0.2 (*2.5)
AuCeSnMA	86.0	5.397 ± 0.003	11.5 ± 1	n.d.

n.d. – gold not detected.

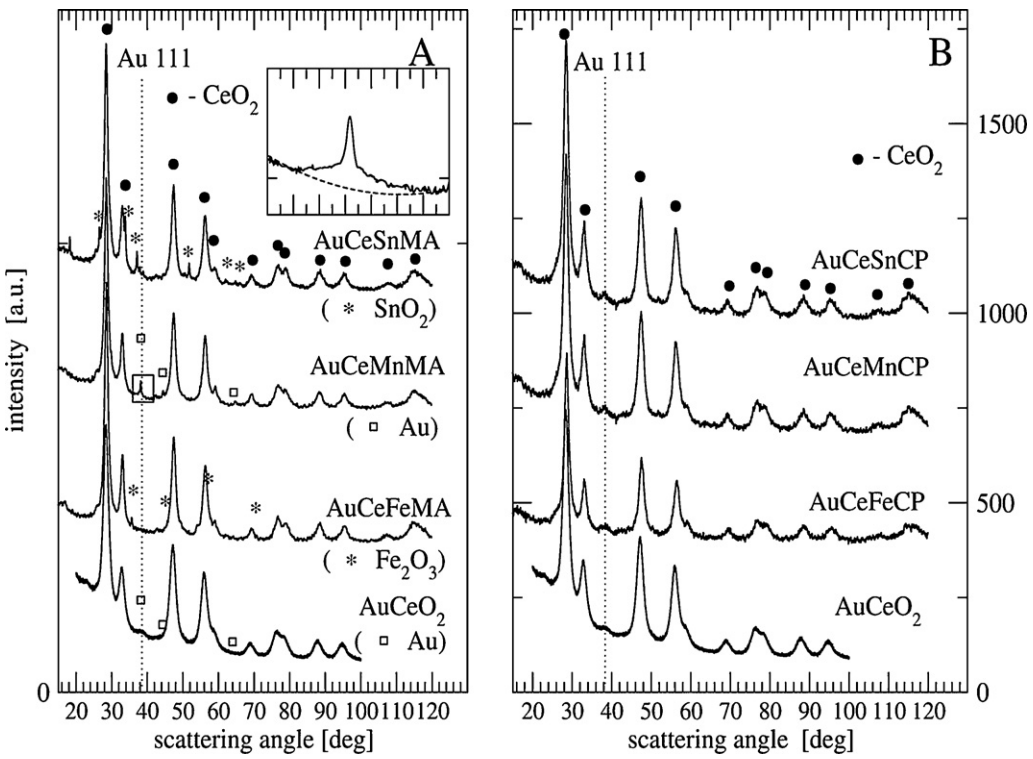

Fig. 1. XRD patterns of the studied catalysts prepared by MA method (A) and by CP method (B); inset in section (A) evidences bimodal distribution of Au particles size in AuCeMnMA sample.

AuCeFeMA and AuCeSnMA samples, a fact that implies very high gold dispersion. In the case of Mn-containing gold catalysts, the routine analysis of XRD patterns supposes gold average particle size much higher than that observed by HRTEM (see below). Close inspection of the XRD pattern suggests however likely modification of the background line (see inset in the Fig. 1) that would correspond to an appearing peak at position close to that of gold pointing to crystallites of 2.9 nm size additionally to 40 nm crystallites (for CP sample) or 25 nm (for MA sample) corresponding to the dominant, narrow peak. As the peak area is proportional to the volume fraction, the number of large crystallites would be 2000 times smaller (CP sample) or 20,000 times smaller (MA sample) than the number of small ones. It is quite likely that such large crystallites may be thus overlooked in HRTEM investigations. Consistency between XRD and TEM results assumes thus bimodal distribution of Au crystal size.

Fig. 2 shows HRTEM images of both MA and CP gold catalysts supported on ceria doped by iron and manganese. The images reveal a complex bulk structure containing distinct randomly distributed crystallites in addition to disordered regions, that can be ascribed to crystal agglomerates not oriented to give diffraction fringes. The roundish particles with higher contrast (appearing as black spots) are gold particles, they are distinguish by difference of contrast. These gold particles are very small and they do not present atomic resolution to measure the lattice parameters. Fig. 3 displays HAADF images of the AuCeFeCP and AuCeMnCP catalysts. Brighter points represent gold nanoparticles. As can be observed, the gold nanoparticles are homogeneously distributed on the support crystals. From this type of images, reliable particle size measurements were made in order to obtain average particle sizes (Table 1) and size distribution histograms (Fig. 4). In all cases, over 700 particles were measured to obtain the average particle size and particle size distribution. The calculations are consistent with XRD data. Looking into the data in Table 1, one cannot find significant differences in the average size of the gold particles in the samples doped by different metal oxides and prepared using the CP and MA methods. It is important to note that on the MA samples the size distribution is large, while on the CP samples it is narrow and centered on 2.5 nm. However, in the MA samples was observed a larger fraction of particles of smaller size (0.5–1.5 nm) in contrast to the samples prepared by coprecipitation. The AuCeFeMA sample manifests fractions of 33 and 22% of 1.5- and 2.5 nm size, respectively, while the matching AuCeFeCP sample shows 12 and 54% distribution of 1.5- and 2.5 nm size, accordingly. Manganese samples display similar allocation: AuCeMnMA–32% (1.5 nm) and 25% (2.5 nm) and AuCeMnCP–14% (1.5 nm) and 46% (2.5 nm).

HRTEM images of Au/CeO_2 evidenced bimodal distribution with presence of both big gold particles (about 10 nm) and highly dispersed gold clusters (about 1 nm). EDS analysis indicated their presence on the surface [5]. The discrepancy between XRD and HRTEM results can be explained by taking into account that the very small gold particles could not be detected by XRD.

The chemical nature of the components formed within the surface region of both CP and MA catalysts was investigated by means of X-ray photoelectron spectroscopy. The Au4f XP spectra of the CP and MA samples, doped by Fe, Mn and Sn, are displayed in Fig. 5 A and the data evaluated from the spectral analysis are summarized in Table 2. The Au4f XP spectra of the samples were fitted successfully with 2–3 components, which can be assigned to differently charged Au nanoparticles. Both electronegative ($Au^{\delta-}$) and electropositive ($Au^{\delta+}$) oxidation states of gold in addition to metallic gold (Au^0) can be distinguished in the $Au4f_{7/2}$ XP spectra. In particular, the main components of Au $4f_{7/2}$ peaks are centred at 84.2 ± 0.2 eV, indicating the presence of gold in metallic state [47–49]. The additional components at binding energy (BE) higher than 84.5 eV are typical of the electropositively charged Au states [47,48]. Higher electropositive Au species were detected in the both Mn-doped gold catalysts. A small amount of the $Au^{\delta-}$ oxidation

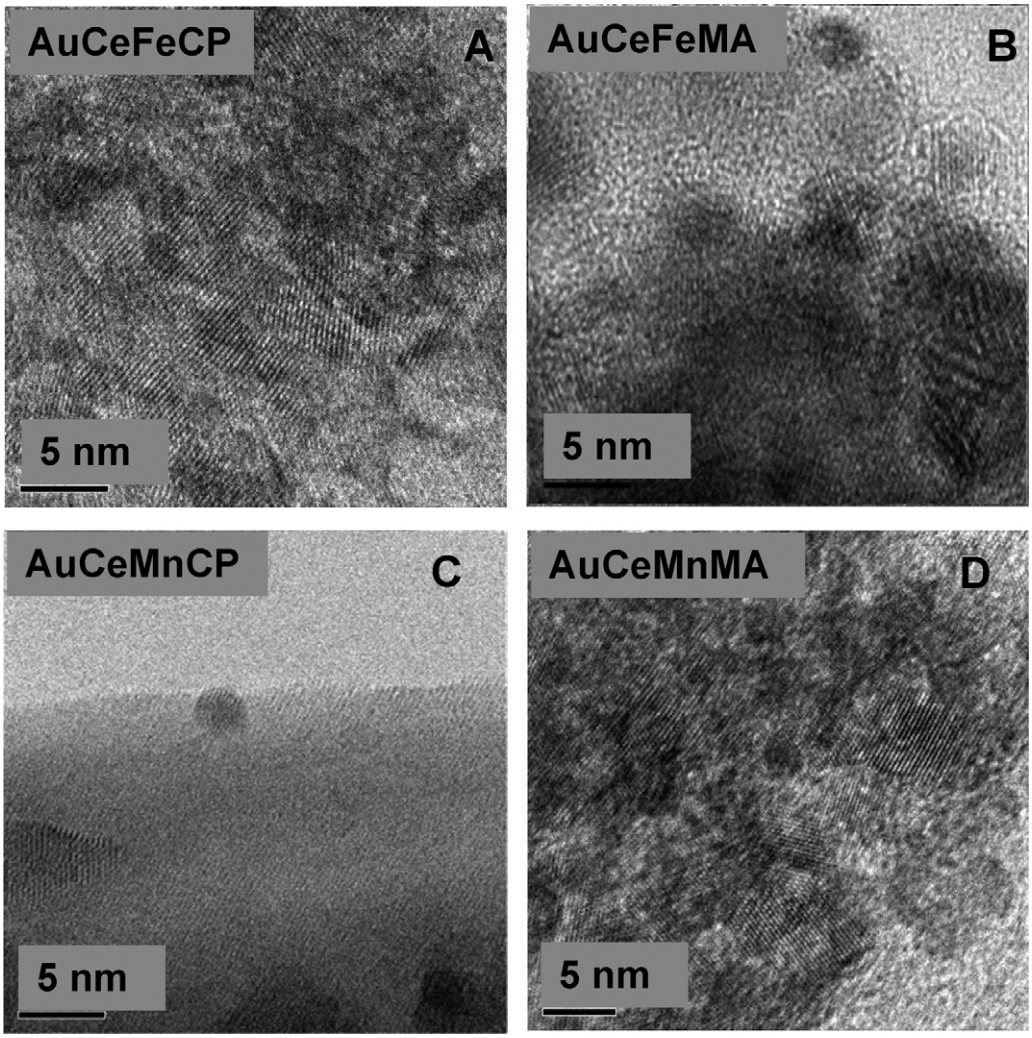

Fig. 2. HRTEM images of the studied catalysts: (A) AuCeFeCP, (B) AuCeFeMA, (C) AuCeMnCP, and (D) AuCeMnMA.

state [50] has been detected in some of samples doped by Mn and Sn.

Ce3d XP spectra of all Me-doped catalysts are collected in Fig. 5 B, where the peaks' assignment is also given. The peaks labelled as u, u′′, u′′′, v, v′′ and v′′′ refer to $3d_{3/2}$ and $3d_{5/2}$, respectively, and are characteristic of Ce(IV) *3d* final states; while u^0, u′, v′ and v^0 refer to $3d_{3/2}$ and $3d_{5/2}$, respectively, and are present for Ce(III) *3d* final state [42]. In all spectra the contribution from both Ce^{4+}

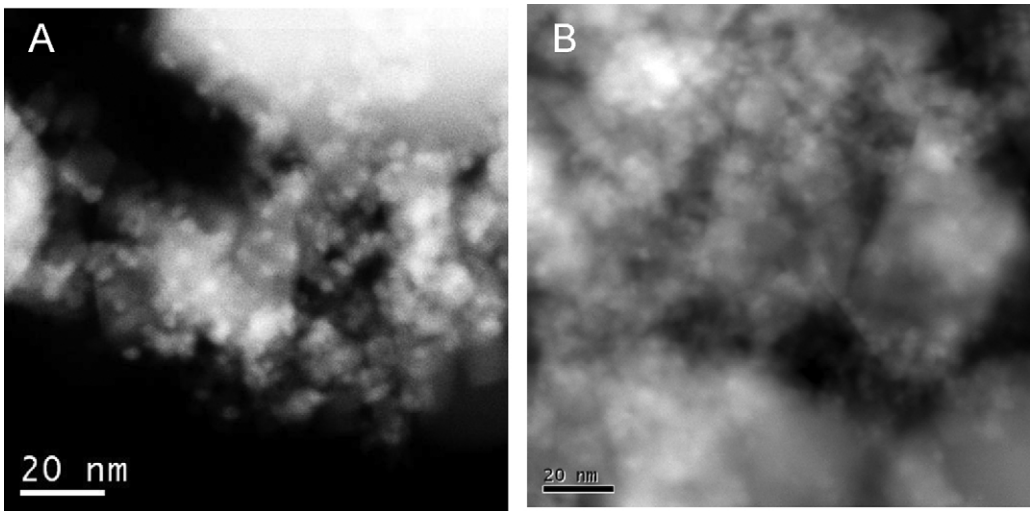

Fig. 3. HAADF images of the AuCeFeCP (A) and AuCeMnCP (B) catalysts.

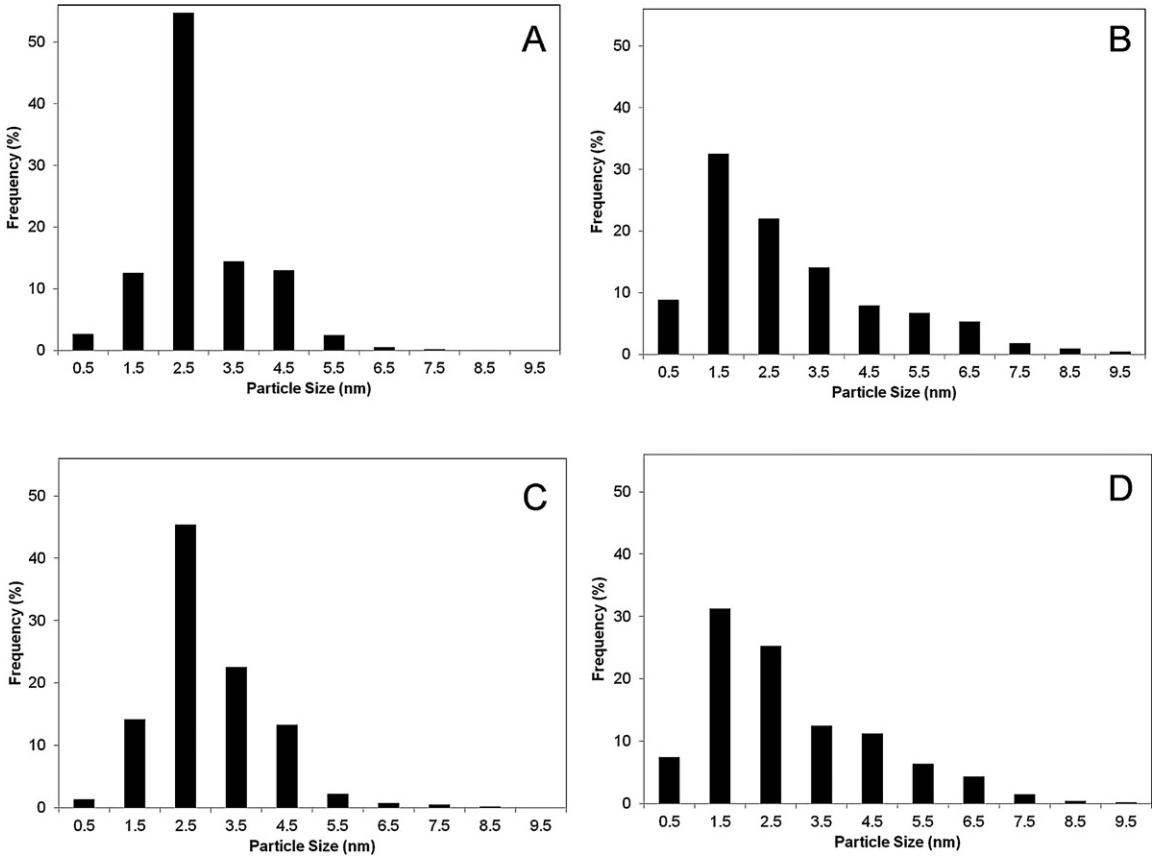

Fig. 4. Size distribution of the gold particles in the studied samples: (A) AuCeFeCP, (B) AuCeFeMA, (C) AuCeMnCP, and (D) AuCeMnMA.

and Ce^{3+} is well visible. In order to make a better insight into the complex character of these spectra we also show the spectrum of the AuCe catalyst. One can see that the behaviour of all the spectra from Me-doped samples, as compared to that of AuCe, is affected by metal oxide dopants. In particular, the differences are related to the main Ce^{3+} peaks at about 885 and 905 eV and they could be better observed in Fig. 5 (C), where the difference spectra are shown. Analyzing the calculated concentration of Ce^{3+} it can be said that this concentration is higher for all MA prepared samples, comparing to that, synthesized by CP (Table 2). Additionally, a high amount of Ce^{3+} ions evaluated from the Ce3d XPS analysis was found with both highly active catalysts, AuCeFeMA and AuCeMnMA.

Table 2
XPS data of the studied samples.

Catalysts	$Au4f_{7/2}$		$Ce3d_{5/2}(Ce^{3+})$	
	Peak position (eV)	(at.%)	Peak position[a] (eV)	(at.%)
AuCe	84.41	0.30	884.66	4.1
	85.51	0.15	881.20	0.9
AuCeFeCP	84.09	0.32	884.21	3.5
	85.30	0.05	881.32	0.6
AuCeFeMA	84.01	0.32	884.15	4.5
	85.67	0.03	881.21	0.9
AuCeMnCP	83.37	0.05	884.45	3.5
	84.40	0.29	881.93	0.7
	85.42	0.18		
AuCeMnMA	84.40	0.29	885.58	7.1
	85.82	0.15	880.70	1.4
AuCeSnCP	83.10	0.05	885.32	4.3
	84.37	0.19	880.44	0.8
	85.42	0.16		
AuCeSnMA	83.00	0.02	884.93	4.7
	84.15	0.26	881.06	1.0
	85.54	0.08		

[a] According to the peak assignment in Fig. 5B, the data for $Ce3d_{5/2}$ peaks refer to v' and v^0.

The XPS analyses reveal also a complex chemical nature of the metal oxide dopants in both the MA and CP samples. Through the $Fe2p_{3/2}$ XPS peaks positioned at 712.1 ± 0.2 and 710.7 ± 0.1 eV for Fe_2O_3 and Fe_3O_4, respectively [51,52], the Fe-containing samples show that iron phases, Fe_2O_3 and small amount Fe_3O_4, coexist in both the CP and MA catalysts. In the Mn-doped samples prepared by CP, only MnO_2 was detected (Mn $2p_{3/2}$ peak positioned at 642.1 eV), while in the MA catalysts both MnO_2 and Mn_3O_4 were registered by the $Mn2p_{3/2}$ peaks at 642.7 and 641.5 eV, respectively [53]. In the Sn-containing samples, SnO_2 was the dominant part ($90 \pm 3\%$) in both the CP and MA samples with the $Sn3d_{5/2}$ peak positioned at 487.1 eV, whereas a small contribution of SnO ($Sn3d_{5/2}$ peak at 485.7 eV) was also registered.

The study of redox properties of the catalysts allow to go further in unravelling the role of different dopants and preparation technique. Fig. 6(A) displays the TPR profiles of the initial supports. It is known that the reduction of ceria proceeds in two steps: reduction of the surface layer at about 500 °C and bulk reduction at a higher temperature (over 800 °C) [53]. As can be seen, the TPR profiles are complex due to the reduction of dopants with different oxidative states in addition to that of ceria. Two TPR peaks with T_{max} at 387 and 590 °C are recorded with CeFeCP support. In the TPR pattern of CeFeMA sample three TPR peaks are observed with T_{max} at 370, 457 and 563 °C, the last one being the most intense. The reduction behaviour of the Fe-doped ceria supports was explained very recently thought detailed analysis of the hydrogen consumption (HC), evaluation of kinetic parameters on the basis of experimental

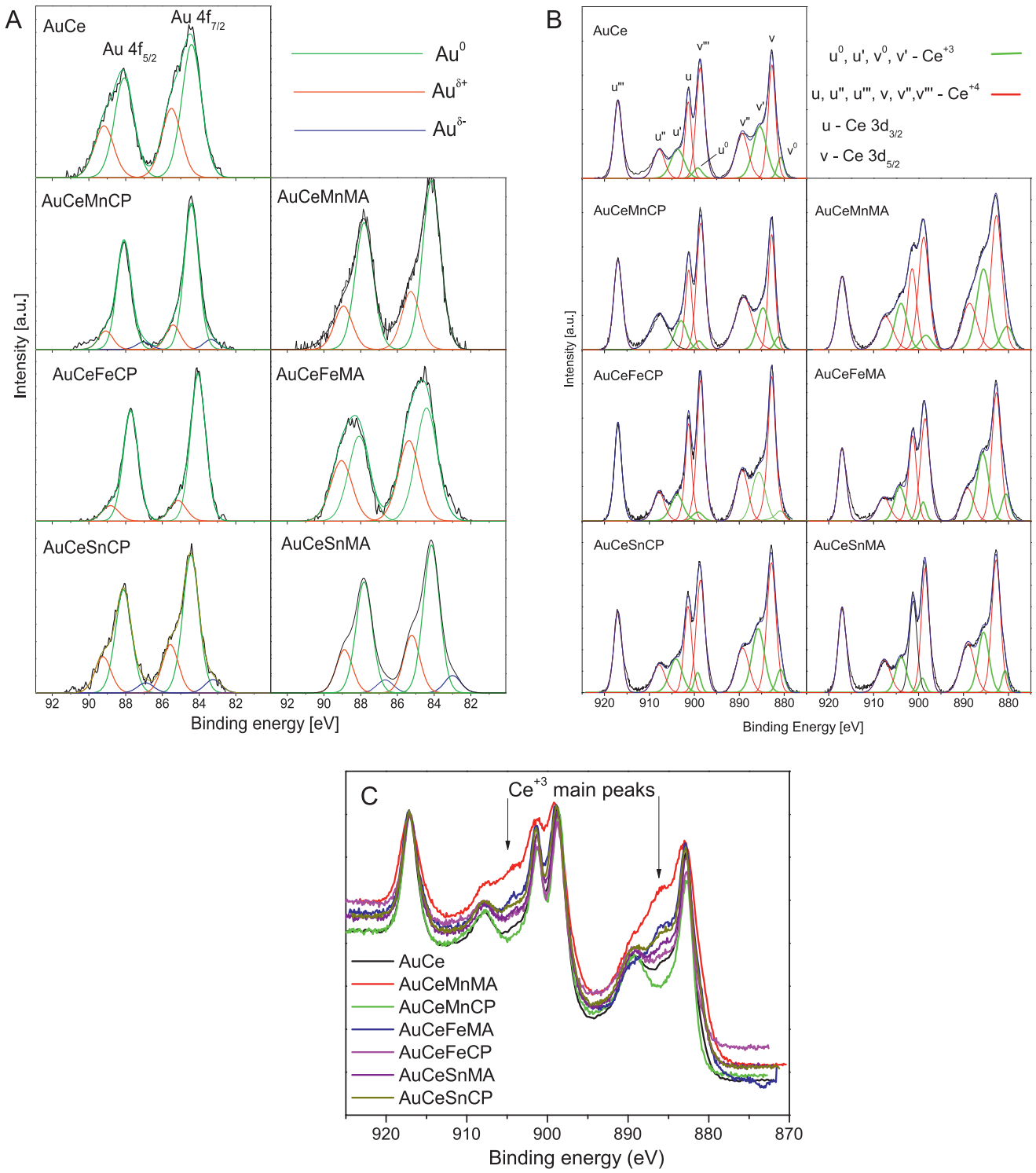

Fig. 5. Experimental and fitted XP spectra of the studied gold catalysts: (A) Au4f spectra; (B) Ce3d spectra and (C) comparison of difference Ce3d XP spectra.

TPR profiles and Mössbauer measurements [54]. The theoretical values of HC for ceria surface layers reduction according to literature data (without effect on the fluorite structure of the grain) is limited to 17% [55] or 20% [56]. In the present case (90 wt% of ceria), the calculated amounts of hydrogen for surface ceria reduction are 0.44 or 0.52 mmol g^{-1}, respectively. The stoichiometric HC for the complete reduction of Fe_2O_3 to Fe^0 (10 wt% of Fe_2O_3) is 1.90 mmol g^{-1} (0.21 mmol g^{-1} for hematite to magnetite and 1.69 mmol g^{-1} for magnetite to metallic iron transformation). Therefore, the theoretical amount of HC for all possible reduction processes is 2.34 or 2.42 mmol g^{-1}. The experimentally obtained HC for CeFeCP support (2.3 mmol g^{-1}) and for CeFeMA (2.2 mmol g^{-1}) means that the state of iron in both initial supports could be considered mainly as Fe^{3+}. Our recent Mössbauer measurements have confirmed that the state of iron in supports synthesized by CP or MA preparation methods is Fe^{3+}, however the Fe-containing phases are different [54]. The quadrupole doublet in the Mössbauer spectra of CeFeCP sample revealed the presence of Fe^{3+} ions incorporated into

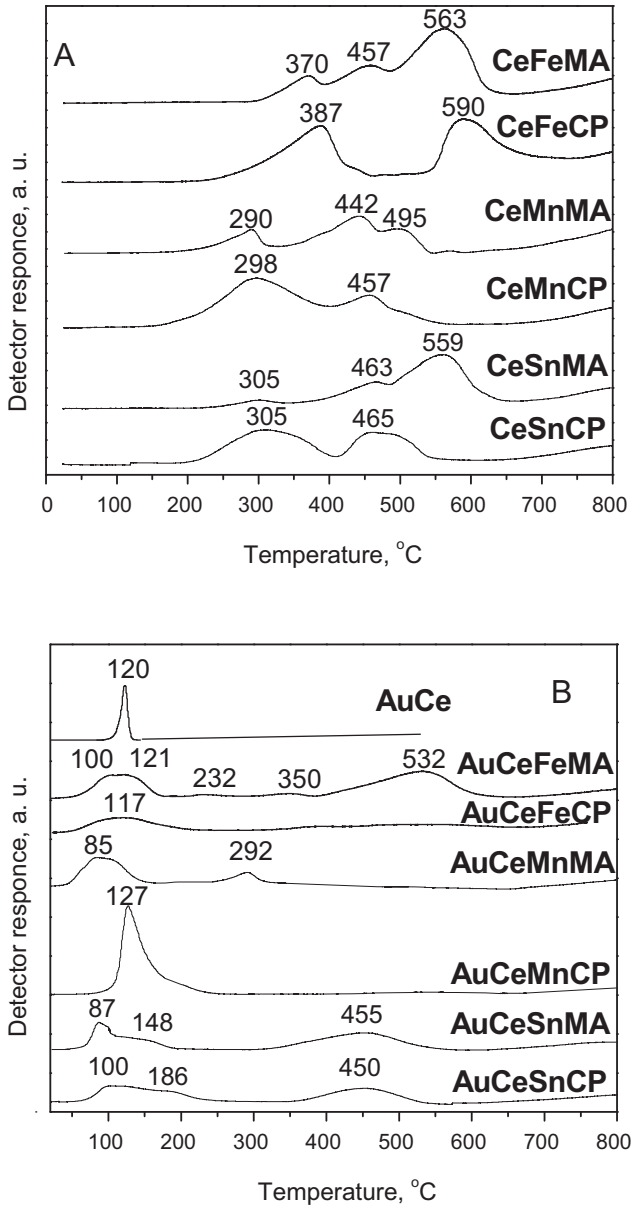

Fig. 6. TPR profiles of the studied samples: (A) initial supports, (B) gold catalysts on ceria modified by Fe, Mn, and Sn, as well on undoped ceria.

ceria (Ce–Fe–O solid solution). The highly intensive sextet component recorded with CeFeMA was assigned to a separate phase of α-Fe_2O_3 (relative weight of 98%) and the low-intensity doublet component (2%) belonged to iron ions in ceria structure. Considering all these results, the first complex TPR peak in the profile of CeFeCP was connected to the reduction of Fe^{3+} to Fe^0. The simulation of the second HT TPR peak by two individual reduction processes allowed to assign the first one to the rest of reduction to Fe^0 and the second process to ceria reduction. The peaks in the profile of the CeFeMA support could be explained with the following reduction processes: $Fe_2O_3 \rightarrow Fe_3O_4 \rightarrow FeO \rightarrow Fe$. The overlapping peaks centred at 563 °C were assigned to two reduction processes; the first one was related to ceria reduction, the second one to metallic Fe^0 formation.

Two TPR peaks with T_{max} at 298 and 457 °C are registered with CeMnCP support, while in the spectra of CeMnMA sample the recorded peaks are characterized with T_{max} at 290, 442 and 495 °C. Two well resolved TPR peaks with T_{max} at 291 and 419 °C were recorded during TPR of bulk MnO_2 oxide (not shown in the figure). According to the literature data the first TPR peak (T_{max} at 291 °C) could be assigned to $MnO_2 \rightarrow Mn_2O_3$ [57] or to $MnO_2/Mn_2O_3 \rightarrow Mn_3O_4$ transition [38], while the second one (T_{max} at 419 °C) is related to $Mn_2O_3 \rightarrow MnO$ [57] or to $Mn_3O_4 \rightarrow MnO$ reduction [38]. Following the above described procedure for calculation of the theoretical amount of HC, the values for Mn containing supports are 1.65 or 1.73 mmol g^{-1} in respect to ceria surface reduction and $MnO_2 \rightarrow Mn_2O_3 \rightarrow MnO$ transformation (1.21 mmol g^{-1} stoichiometric HC needed for reduction of 10 wt%. of dopant as MnO_2). The comparison with the experimental values (1.60 mmol g^{-1} for CeMnCP and 1.24 mmol g^{-1} for CeMnMA), implies that with CP support the most probable oxidative state of dopant ions is Mn^{4+}, however with MA one the predominant oxidative state could not be Mn^{4+}. Taking into consideration the stoichiometric HC for $Mn_2O_3 \rightarrow MnO$ reduction (0.93 mmol g^{-1}), the presence of Mn^{3+} ions could be supposed in the case of MA preparation mode.

Table 3
Hydrogen consumption corresponding to the first TPR peak of the catalysts (temperature interval up to 250 °C).

Samples	Hydrogen consumption (mmol g^{-1})
AuCe	0.46
AuCeFeCP	0.56
AuCeFeMA	0.71
AuCeMnCP	1.62
AuCeMnMA	0.76
AuCeSnCP	0.69
AuCeSnMA	0.61

In the profile of CeSnCP are observed two TPR peaks with T_{max} at 305 and 465 °C. In this case, the possible transition of dopant phase is $SnO_2 \rightarrow SnO$. The stoichiometric HC for the reduction of SnO_2 to SnO (10 wt% of SnO_2) is 0.66 mmol g^{-1}. Therefore, the theoretical amount of HC for ceria surface reduction and reduction of dopant is 1.10–1.18 mmol g^{-1}. The experimentally obtained HC for CeSnCP support (1.08 mmol g^{-1}) and for CeSnMA (1.20 mmol g^{-1}) coincide well with theoretical values and revealed that the state of tin in both initial supports could be considered mainly as Sn^{4+}. In agreement with data, reported by Pavelko et al., the peak at 305 °C can be attributed to the reduction of surface of SnO_2, while the bulk reduction of SnO_2 is observed at higher temperature (>500 °C) [58]. In present case the peak at 465 °C is complex and includes also surface reduction of CeO_2. Considering high intensity of the first reduction peak (at 305 °C) in the profile of CeSnCP it is possible to hypothesize that partial surface ceria reduction occurs also at lower temperature, due to the improved oxygen mobility after the doping. The peak at 305 °C is very weak in the profile of CeSnMA, while in the second broad and complex peak two maxima at 463 and 559 °C are well distinguishable. Very low intensity of the peak at 305 °C could be related to hampered surface reduction of separate SnO_2 phase, due to applied preparation method. The broad intense peak at at 559 °C with well defined shoulder (T_{max} = 463 °C) can be ascribed to ceria surface reduction and reduction of SnO_2 to SnO.

In Fig. 6(B) are shown the TPR profiles of the gold containing catalysts. Comparing the TPR profiles of the Au-containing samples with the initial supports it is seen that in all cases the addition of gold causes a significant lowering of the reduction temperature. All low temperature (LT) peaks are assigned to the reduction of ceria surface layers as well as to the reduction of the corresponding dopant in the support. Positively charged gold is also reduced but this process is negligible against the background of other reduction developments. The LT peaks of the Au-containing catalysts are in the temperature interval up to 250 °C and HC was calculated based on the TPR peaks in this temperature range. The results are listed in Table 3. An effect of increased HC is registered for all gold catalysts

on doped-ceria by comparison with gold supported on undoped ceria. The reduction behavior is strongly influenced by the preparation method and the nature of dopant. The hydrogen consumption is higher with the CP-prepared Mn- and Sn-doped Au/ceria catalysts than that with the corresponding MA entities. An opposite effect is observed with Fe-containing gold catalysts, i.e. higher HC is registered with the MA sample. The first LT peak in the TPR profile of the AuCeFeMA catalyst is complex with two maxima at 100 and 121 °C. This peak was assigned to the gold-enhanced reduction of ceria surface layers and to the reduction of separate hematite phase. An important conclusion was drawn, that the reduction of hematite to magnetite (about 40%) at relatively very low temperature (T_{max} = 121 °C) was not resulted only from the presence of finely dispersed gold particles. Our previous TPR experiments have demonstrated significant shift to lower temperature of hematite to magnetite transformation over Au/Fe_2O_3 comparing to α-Fe_2O_3 but with T_{max} at about 280 °C [59]. In addition to the effect of gold, it was assumed that the reduction of the hematite phase, especially at the border with ceria, was significantly enhanced because of higher ionic conductivity of ceria after modification with Fe by MA method. In the TPR profile of AuCeFeCP catalyst was registered single peak at 117 °C. In this case, the preparation method facilitates formation of CeO_2-like solid solution and participation of iron ions in reduction process is hampered. On the basis of structural differences of both Fe-doped ceria supports this peak was related only to the surface ceria layer reduction. The existence of separate Fe-containing phase, able to undergo reduction at relatively very low temperature, allows reasonably explaining higher HC of AuCeFeMA catalyst in comparison with AuCeFeCP.

In the spectra of AuCeMnCP catalyst only one intense LT TPR peak with T_{max} = 127 °C was present. For AuCeMnMA sample the recorded peaks were characterized with T_{max} at 85 °C and a second less intense peak at T_{max} = 292 °C. Looking at Table 3, the calculated HC for the AuCeMnCP catalyst is a sum of HC for ceria surface reduction and HC for the $MnO_2 \rightarrow Mn_2O_3 \rightarrow MnO$ transformation. This result could be interpreted with increased mobility of oxygen due to insertion of Mn ions in ceria cell. In contrast, the reduction of separate manganese phase in AuCeMnMA sample is slightly affected.

Two broad and complex peaks were observed in the LT-TPR profiles of gold on Sn-doped ceria catalysts. The peaks displayed T_{max} at 87 and 148 °C for AuCeSnMA, and at 100 and 186 °C for AuCeSnCP samples. By analogy with above commented results, it could be hypothesized that these peaks are associated with gold-enhanced reduction of ceria surface layers and with transition $SnO_2 \rightarrow SnO$.

The analysis of reduction behaviour well agrees with the XPS data evidencing the dominant initial oxidation state of the dopants being as in Fe_2O_3, MnO_2 and SnO_2.

3.2. Activity and stability in the water–gas shift reaction

Fig. 7 illustrates the temperature dependence of the CO conversion during the WGSR over gold catalysts supported on doped CeO_2, as well on pure CeO_2. Generally, the catalytic activities of the MA catalysts were found to be higher than those of the corresponding CP samples. Such behaviour we have already observed for the gold catalysts supported on ceria doped by Al and RE metals [23–26]. In these papers we have reported that metals exhibiting an oxidation state different to that of cerium in ceria (+4) modify the crystal structure of the latter and cause the formation of oxygen vacancies. Many authors indicate the crucial role of the oxygen vacancies as an important factor that enhances the catalytic activity of the gold/ceria catalysts [11,60]. On the other hand, the catalyst stability is also affected by a doping metal, which prevents agglomeration of the gold and ceria particles in the ceria crystal structure [23,24]. For the present samples, the differences in WGS activity

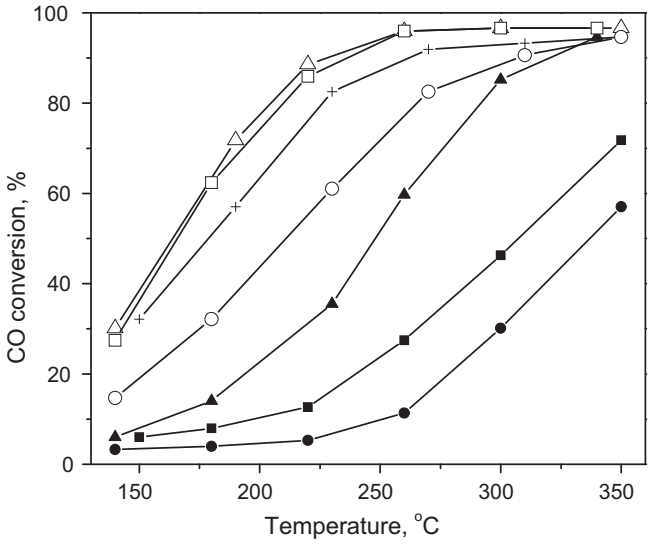

Fig. 7. Temperature dependence of the CO conversion over the studied catalysts: (+)–AuCe; (△) – AuCeFeMA; (▲) – AuCeFeCP; (□)–AuCeMnMA; (■)–AuCeMnCP; (○)–AuCeSnMA; (●)–AuCeSnCP.

between the MA and CP samples are significant and similar to gold catalysts based on ceria-alumina [23–25]. The MA catalysts, doped by Fe and Mn, manifested higher WGS activity than the undoped Au/ceria sample and the sample doped by Sn.

The order of WGS activities at 250 °C of the present catalysts is the following:

AuCeFeMA≈AuCeMnMA > AuCe > AuCeSnMA > AuCeFeCP > AuCeMnCP > AuCeSnCP.

As we already mentioned, the coprecipitation technique leads to bulk modification of a catalyst by a doping metal, while the MA method causes only a surface modification. This could explain the higher catalytic activity of the MA samples than that of the CP entities, because during the catalytic reaction the oxidation capacity of water is sufficient to reoxidise only the oxygen vacancies at the surface. It is likely that a faster reoxidation of the catalyst surface by the water vapour implicates a higher activity of the MA catalysts during the reaction process. Another explanation of the higher activity should be associated with the presence of separate dopant's phase, which is caused by the specific character of the MA method. Being in close contact with gold these reducible dopants could also act as a co-catalyst and exhibit activity in the WGS reaction due to their own redox behaviour. In preceding paper [61] we have reported that Au/iron oxide catalyst is very active in the same reaction. Thus analyzing the high activity of the Au-containing catalysts supported on Fe-doped ceria, we should also consider that the possible reaction activity originated from both the Au/Fe-oxide and Au/Ce-oxide phases. We suppose that in this case probably an additive effect of activities is provided. This suggestion can be confirmed by the higher WGS activity established in this work compared to the activity of Au supported on alumina-doped ceria, which is not active in the WGS reaction [25]. Gold catalysts containing Sn, the latter having also variable oxidation state, exhibited a lower activity than those containing Fe or Mn. The explanation of this experimental result could be based on the calculation of Au to Me ratios (Me = Fe, Mn, Sn) by XPS. The obtained data were as follows: 0.3390 (AuCeFeCP), 0.7577 (AuCeFeMA), 0.1728 (AuCeMnCP), 1.5363 (AuCeMnMA), 0.0380 (AuCeSnCP), and 0.0594 (AuCeSnMA). The analysis revealed that higher values are obtained in the case of Fe or Mn doping of ceria. This result correlates with catalytic activity order. The lowest values for Au/Sn ratio could explain the insignificant additive contribution of Au/Sn-oxide

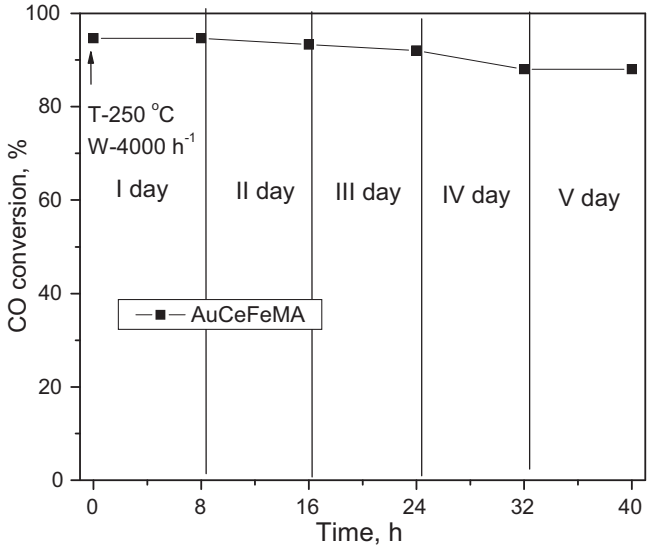

Fig. 8. Stability test with the AuCeFeMA catalyst, based on CO conversions at 250 °C and GHSV = 4000 h^{-1} within 40 h (8 h a day for a period of 5 days - during pauses, the reaction mixture was kept at room temperature).

phase, which reflects on the total WGS activity of Sn-doped gold catalysts.

Following the aim of present study, i.e. to reveal the effect of the preparation method and the type of dopant for ceria support modification on the WGS activity of the resulting gold catalysts, we gave emphasis on the different nature of the support materials. However, the cooperation between the gold nanoparticles and the support during the catalytic cycle should be rationalized in order to explain the variations in the catalytic activity. According to the conclusions derived from the analysis of the HRTEM images, in the MA samples was detected a larger fraction of particles of smaller size in contrast to the samples prepared by coprecipitation. These data in combination with high amount of Ce^{3+} ions evaluated from the Ce3d XP spectra of both highly active catalysts, AuCeFeMA and AuCeMnMA, are very informative bearing in mind our suggestion for the active sites over gold/ceria catalysts in the WGS reaction, namely AuV_oCe^{3+} (V_o – oxygen vacancy), where the co-existence of both small gold nanoparticles and Ce^{3+} in close contact is decisive [25,26,62]. In the case of iron and manganese oxides, which are also active as supports for the WGS reaction, it could be suggested that AuV_oMe^{n-1} (Me = Fe or Mn, n–valence of the metal dopant) may also be an active site for the WGS reaction. The doping metal oxide plays not only the role of structural promoter but it is also an active phase increasing the WGS activity. As concerns Sn-doped samples, in particular AuCeSnCP, a discrepancy exists between high atomic concentrations of Ce^{3+} from XPS analysis (that is comparable to that of the most active samples) and the catalytic behaviour. We suggest that in this case Ce^{3+} formation is influenced by Sn^{2+} oxidation to Sn^{4+}, which was found to be the dominant oxidation state of tin. This suggestion is consistent with the results of Scala et al. that have evidenced by XPS phase transition from Ce^{4+} to Ce^{3+} accompanied by the oxidation of Sn after tin deposition on the CeO_2 surface [63].

Along with the discussion of structure-reactivity relationship, another important point is the catalysts' resistance towards deactivation. A 40 h catalytic test at 250 °C over the most active AuCeFeMA sample showed good stability of the catalyst (Fig. 8). An insignificant deactivation (about 7%) was observed, considering the difference between 94.7% and 88.2% CO conversion at the start and the end of the stability test, respectively. It is important to note that this slow deactivation was reversible. The same WGS activity in the whole temperature range was observed after reoxidation at 200 °C in air for 60 min, suggesting that the reason for the observed slight loss of activity cannot be associated with agglomeration of the gold or carrier particles. The most probable reason could be blocking of the active sites by carbon-containing species.

Finally, analyzing the effect of Fe and Mn ions addition to ceria, as well of preparation method, it could be concluded that suitable chemical composition and synthesis route allow the development of gold catalysts of good WGS performance that can be very promising for practical application.

4. Conclusions

The effect of different preparation methods and of the nature of dopants on the WGS activity of gold catalysts supported on ceria modified by various metal oxides (Me = Fe, Mn and Sn) was studied. The catalysts prepared by mechanochemical activation exhibited a higher activity than those prepared using a coprecipitation route of synthesis. The characterization results revealed that the CP method leads to bulk modification of the catalysts by a doping metal, while the MA method causes only a surface modification. High and stable WGS activity of the catalysts based on ceria modified by Fe and Mn has been established. TPR results prove a higher oxygen capacity than that of the gold catalyst on undoped ceria and this effect is stronger in the MA samples. Oxygen capacity is affected by the use of various preparation techniques as well as by the nature of dopant. The presence of gold particles with smaller size and a high concentration of the Ce^{3+} ions, registered in the highly active catalysts containing Fe or Mn, is in agreement with our proposed model of the active sites for the WGS reaction [3]. In addition to the active sites originated from Ce oxide (AuV_oCe^{3+}), the active sites formed after doping, AuV_oMe^{n-1} (Me = Fe or Mn), should also contribute to the WGS activity.

Acknowledgements

T. Tabakova is grateful for the financial support via Bulgarian project "Science and business" (BG051PO001-3.3-05/0001) (contract DO2-563) funded by "Human Resources Development" Operational Programme (financed by the European Social Fund). This work has been performed in the framework of the NATO Project CLG 984160 and COST Action CM0903/02. R. Zanella acknowledges PAPIIT IN108310 and CONACYT130407 projects for financial support.

References

[1] Q. Fu, A. Weber, M. Flytzani-Stephanopoulos, Catalysis Letters 77 (2001) 87–95.
[2] D. Andreeva, V. Idakiev, T. Tabakova, L. Ilieva, P. Falaras, A. Bourlinos, A. Travlos, Catalysis Today 72 (2002) 51–57.
[3] Q. Fu, S. Kudriavtseva, H. Saltsburg, M. Flytzani-Stephanopoulos, Chemical Engineering Journal 93 (2003) 41–53.
[4] A. Luengaruemitchai, S. Osuwan, E. Gulabi, Catalysis Communications 4 (2003) 215–221.
[5] T. Tabakova, F. Boccuzzi, M. Manzoli, J.W. Sobczak, V. Idakiev, D. Andreeva, Applied Catalysis B 49 (2004) 73–81.
[6] H. Sakurai, T. Akita, S. Tsubota, M. Kiuchi, M. Haruta, Applied Catalysis A 291 (2005) 179–187.
[7] Q. Fu, W. Deng, H. Saltsburg, M. Flytzani-Stephanopoulos, Applied Catalysis B 56 (2005) 57–68.
[8] W. Deng, C. Carpenter, N. Yi, M. Flytzani-Stephanopoulos, Topics in Catalysis 44 (2007) 199–208.
[9] G. Jacobs, S. Ricote, P.M. Patterson, U.M. Graham, A. Dozier, S. Khalid, E. Rhodus, B.H. Davis, Applied Catalysis A 292 (2005) 229–243.
[10] Ch. H. Kim, L.T. Thompson, Journal of Catalysis 230 (2005) 66–74.
[11] D. Tibiletti, A. Amieiro-Fonseca, R. Burch, Y. Chen, J.M. Fisher, A. Goguet, C. Hardacre, P. Hu, D. Thompsett, Journal of Physical Chemistry B 109 (47) (2005) 22553–22559.
[12] G.C. Bond, C. Louis, D.T. Thompson, Catalysis by Gold, Imperial College Press, UK, 2006.
[13] R. Burch, Physical Chemistry Chemical Physics 8 (2006) 5483–5500.
[14] R. Leppelt, B. Schumacher, V. Plzak, M. Kinne, R.J. Behm, Journal of Catalysis 244 (2006) 137–152.

[15] A. Karpenko, R. Leppelt, V. Plzak, J. Cai, A. Chuvilin, B. Schumacher, U. Kaiser, R.J. Behm, Topics in Catalysis 44 (2007) 183–198.
[16] A. Karpenko, Y. Denkwitz, V. Plzak, J. Cai, R. Leppelt, B. Schumacher, R.J. Behm, Catalysis Letters 116 (2007) 105–115.
[17] H. Daly, J. Ni, D. Thompsett, F.C. Meunier, Journal of Catalysis 254 (2008) 238–243.
[18] A. Abd El-Moemen, A. Karpenko, Y. Denkwitz, R.J. Behm, Journal of Power Sources 190 (2009) 64–75.
[19] M. Boaro, M. Vicario, J. Llorca, C. de Leitenburg, G. Dolcetti, A. Trovarelli, Applied Catalysis B 88 (2009) 272–282.
[20] C. Galletti, S. Specchia, G. Saracco, V. Specchia, Topics in Catalysis 52 (2009) 688–692.
[21] B.A. Lenite, C. Galletti, St Specchia, International Journal of Hydrogen Energy 36 (13) (2011) 7750–7758.
[22] A.E.C. Palmqvist, E.M. Johansson, S.G. Jaras, M. Muhammed, Catalysis Letters 56 (1998) 69–75.
[23] D. Andreeva, I. Ivanov, L. Ilieva, M.A. Abrashev, Applied Catalysis A 302 (2006) 127–133.
[24] D. Andreeva, I. Ivanov, L. Ilieva, J.W. Sobczak, G. Avdeev, T. Tabakova, Applied Catalysis A 333 (2007) 153–160.
[25] D. Andreeva, I. Ivanov, L. Ilieva, J.W. Sobczak, G. Avdeev, K. Petrov, Topics in Catalysis 44 (2007) 173–182.
[26] D. Andreeva, I. Ivanov, L. Ilieva, M.V. Abrashev, R. Zanella, J.W. Sobczak, W. Lisowski, M. Kancheva, G. Avdeev, K. Petrov, Applied Catalysis A 357 (2009) 159–169.
[27] P. Konova, A. Naydenov, C. Venkov, D. Mehandjiev, D. Andreeva, T. Tabakova, Journal of Molecular Catalysis A: Chemical 213 (2004) 235–240.
[28] Y. Denkwitz, A. Karpenko, V. Plzak, R. Leppelt, B. Schumaher, R.J. Behm, Journal of Catalysis 246 (2007) 74–90.
[29] Y. Hao, M. Mihaylov, E. Ivanova, K. Hadjiivanov, H. Knozinger, Journal of Catalysis 261 (2009) 137–149.
[30] A. Abd El-Moemen, G. Kucerova, R.J. Behm, Applied Catalysis B 95 (2010) 57–70.
[31] X. Wang, R.J. Gorte, Applied Catalysis A 247 (2003) 157–162.
[32] T. Tabakova, M. Manzoli, D. Paneva, F. Boccuzzi, V. Idakiev, I. Mitov, Applied Catalysis B 101 (2011) 266–274.
[33] T. Tabakova, G. Avgouropoulos, J. Papavasiliou, M. Manzoli, F. Boccuzzi, K. Tenchev, F. Vindigni, T. Ioannides, Applied Catalysis B 101 (2011) 256–265.
[34] A. Penkova, K. Chakarova, O.H. Laguna, K. Hadjiivanov, F. Romero Saria, M.A. Centeno, J.A. Odriozola, Catalysis Communications 10 (2009) 1196–1202.
[35] O.H. Laguna, M.A. Centeno, G. Arzamendi, L.M. Gandía, F. Romero-Sarria, J.A. Odriozola, Catalysis Today 157 (2010) 155–159.
[36] L. Ilieva, G. Pantaleo, I. Ivanov, A. Maximova, R. Zanella, Z. Kaszkur, A.M. Venezia, D. Andreeva, Catalysis Today 158 (2010) 44–55.
[37] L.C. Wang, X.S. Huang, Q. Liu, Y.M. Liu, Y. Cao, H.Y. He, K.N. Fan, J.H. Zhuang, Journal of Catalysis 259 (2010) 66–74.
[38] Y.B. Tu, J.Y. Luo, M. Meng, G. Wang, J.J. He, International Journal of Hydrogen Energy 34 (2009) 3743–3754.
[39] S. Wang, J. Huang, Y. Zhao, S. Wang, X. Wang, T. Zhang, S. Wu, S. Zhang, W. Huang, Journal of Molecular Catalysis A 259 (2006) 245–252.
[40] M. Romeo, K. Bak, J. El Fallah, F. Le Normand, L. Hilaire, Surface and Interface Analysis 20 (1993) 508–512.
[41] L. Armelao, D. Barecca, G. Bottaro, A. Gasparotto, E. Tondello, Surface Science Spectra 8 (2001) 247–249.
[42] A.Q. Wang, P. Punchaipetch, R.M. Wallace, T.D. Golden, Journal of Vacuum Science and Technology B 21 (2003) 1169–1175.
[43] N. Kotzev, D. Shopov, Journal of Catalysis 22 (1971) 297–301.
[44] D.A.M. Monti, A. Baiker, Journal of Catalysis 83 (1983) 323–335.
[45] H. Bao, X. Chen, J. Fang, Z. Jiang, W. Huang, Catalysis Letters 125 (2008) 160–167.
[46] E.J. Mittemeijer, P. Scardi (Eds.), Diffraction Analysis of the Microstructure of Materials, Springer Series in Material Science, vol. 68, Springer-Verlag, Berlin Heidelberg, 2004.
[47] J.F. Moulder, W.F. Stickle, P.E. Sobol, K.D. Bomben, Handbook of X-ray Photoelectron Spectroscopy, Physical Electronics, Chanhassen USA, 1995.
[48] A.M. Venezia, G. Pantaleo, A. Longo, G. Di Carlo, M.P. Casaletto, L.F. Liotta, G. Deganello, Journal of Physical Chemistry B 109 (2005) 2821–2827.
[49] L.F. Liotta, G. Di Carlo, A. Longo, G. Pantaleo, A.M. Venezia, Catalysis Today 139 (2008) 174–179.
[50] S. Shukla, S. Seal, Nanostructured Materials 11 (1999) 1181–1193.
[51] A. De Stefanis, S. Kaciulis, L. Pandolfi, Microporous Mesoporous Materials 99 (2007) 140–148.
[52] NIST X-ray Photoelectron Spectroscopy Database. V. 4.0, 2008, (http://srdata.nist.gov/xps/).
[53] H.C. Yao, Y.F. Yu Yao, Journal of Catalysis 86 (1984) 254–265.
[54] L. Ilieva, G. Munteanu, P. Petrova, T. Tabakova, N. Velinov, I. Mitov, Reaction Kinetics, Mechanisms, and Catalysis 105 (2012) 39–52.
[55] M.G. Sanchez, J.L. Gazquez, Journal of Catalysis 104 (1987) 120–135.
[56] A. Laachir, V. Perrichon, A. Bardi, J. Lamotte, E. Catherine, J.C. Lavalley, J. El Faallah, L. Hilaire, F. le Normand, E. Quemere, G.N. Sauvion, O. Touret, Journal of the Chemical Society, Faraday Transactions 87 (1991) 1601–1609.
[57] E.R. Stobe, B.A. De Boer, J.W. Geus, Catalysis Today 47 (1999) 161–167.
[58] R.G. Pavelko, A.A. Vasiliev, E. Llobet, X. Vilanova, N. Barrabés, F. Medina, V.G. Sevastyanov, Sensors and Actuators B 137 (2009) 637–643.
[59] L. Ilieva, D. Andreeva, A. Andreev, Thermochimica Acta 292 (1997) 169–174.
[60] X. Wang, J.A. Rodrigues, J.C. Hanson, M.P. Perez, J. Evans, Journal of Chemical Physics 123 (2005) 221101–221106.
[61] D. Andreeva, V. Idakiev, T. Tabakova, A. Andreev, Journal of Catalysis 158 (1996) 354–355.
[62] D. Andreeva, M. Kantcheva, I. Ivanov, L. Ilieva, J.W. Sobczak, W. Lisowski, Catalysis Today 158 (2010) 69–77.
[63] T. Skala, F. Sutara, K.C. Prince, V. Matolin, Journal of Electron Spectroscopy and Related Phenomena 169 (2009) 20–25.